



RESEARCH

Open Access



Developing a medical device-grade T_2 phantom optimized for myocardial T_2 mapping by cardiovascular magnetic resonance

Constantin-Cristian Topriceanu^{1,2,5†} , Massimiliano Fornasiero^{3†}, Han Seo⁴, Matthew Webber^{1,2,4,5}, Kathryn E. Keenan⁶, Karl F. Stupic⁶, Rüdiger Bruehl⁷, Bernd Ittermann⁷, Kirsty Price⁸, Louise McGrath⁸, Wenjie Pang⁹, Alun D. Hughes^{2,5}, Reza Nezafat¹⁰, Peter Kellman¹¹, Iain Pierce^{1,2}, James C. Moon^{1,2} and Gabriella Captur^{2,4,5,12*} 

Abstract

Introduction A long T_2 relaxation time can reflect oedema, and myocardial inflammation when combined with increased plasma troponin levels. Cardiovascular magnetic resonance (CMR) T_2 mapping therefore has potential to provide a key diagnostic and prognostic biomarkers. However, T_2 varies by scanner, software, and sequence, highlighting the need for standardization and for a quality assurance system for T_2 mapping in CMR.

Aim To fabricate and assess a phantom dedicated to the quality assurance of T_2 mapping in CMR.

Method A T_2 mapping phantom was manufactured to contain 9 T_1 and T_2 ($T_1|T_2$) tubes to mimic clinically relevant native and post-contrast T_2 in myocardium across the health to inflammation spectrum (i.e., 43–74 ms) and across both field strengths (1.5 and 3 T). We evaluated the phantom's structural integrity, B_0 and B_1 uniformity using field maps, and temperature dependence. Baseline reference $T_1|T_2$ were measured using inversion recovery gradient echo and single-echo spin echo (SE) sequences respectively, both with long repetition times (10 s). Long-term reproducibility of $T_1|T_2$ was determined by repeated $T_1|T_2$ mapping of the phantom at baseline and at 12 months.

Results The phantom embodies 9 internal agarose-containing $T_1|T_2$ tubes doped with nickel di-chloride (NiCl_2) as the paramagnetic relaxation modifier to cover the clinically relevant spectrum of myocardial T_2 . The tubes are surrounded by an agarose-gel matrix which is doped with NiCl_2 and packed with high-density polyethylene (HDPE) beads. All tubes at both field strengths, showed measurement errors up to ≤ 7.2 ms [$< 14.7\%$] for estimated T_2 by balanced steady-state free precession T_2 mapping compared to reference SE T_2 with the exception of the post-contrast tube of ultra-low T_1 where the deviance was up to 16 ms [40.0%]. At 12 months, the phantom remained free of air bubbles, susceptibility, and off-resonance artifacts. The inclusion of HDPE beads effectively flattened the B_0 and B_1 magnetic fields in the imaged slice. Independent temperature dependency experiments over the 13–38 °C range confirmed the greater stability of shorter vs longer $T_1|T_2$ tubes. Excellent long-term (12-month) reproducibility of measured $T_1|T_2$ was demonstrated across both field strengths (all coefficients of variation $< 1.38\%$).

[†]Constantin-Cristian Topriceanu and Massimiliano Fornasiero Joint 1st authors

*Correspondence:

Gabriella Captur

gabriella.captur@ucl.ac.uk

Full list of author information is available at the end of the article



© The Author(s) 2023. **Open Access** This article is licensed under a Creative Commons Attribution 4.0 International License, which permits use, sharing, adaptation, distribution and reproduction in any medium or format, as long as you give appropriate credit to the original author(s) and the source, provide a link to the Creative Commons licence, and indicate if changes were made. The images or other third party material in this article are included in the article's Creative Commons licence, unless indicated otherwise in a credit line to the material. If material is not included in the article's Creative Commons licence and your intended use is not permitted by statutory regulation or exceeds the permitted use, you will need to obtain permission directly from the copyright holder. To view a copy of this licence, visit <http://creativecommons.org/licenses/by/4.0/>. The Creative Commons Public Domain Dedication waiver (<http://creativecommons.org/publicdomain/zero/1.0/>) applies to the data made available in this article, unless otherwise stated in a credit line to the data.

Conclusion The T_2 mapping phantom demonstrates excellent structural integrity, B_0 and B_1 uniformity, and reproducibility of its internal tube $T_1|T_2$ out to 1 year. This device may now be mass-produced to support the quality assurance of T_2 mapping in CMR.

Keywords T_1 mapping, T_2 mapping, Phantom, Quality control

Introduction

Cardiovascular magnetic resonance (CMR) allows noninvasive myocardial tissue characterization. Fully quantitative T_2 mapping techniques expose not only regionality, but also diffuse changes in T_2 , offering the prospect of redefining disease (disease vs. normal) and monitoring interval change. However, the measured T_2 values differ by parameters such as temperature, field strength, type of scanner and CMR sequence. The lack of protocol standardization has hampered the definition of myocardial T_2 ranges in health, the pooling of multi-center mapping data into generalizable outputs, and the robust conduct of longitudinal studies that serially measure T_2 . The Society for Cardiovascular Magnetic Resonance (SCMR)'s current recommendation is to perform stratified statistical analysis to adjust for site scan characteristics [1]. However, as a first step towards better standardization, an internationally accepted reference object for CMR T_2 mapping is desirable [2].

In clinical practice, myocardial T_2 can vary with age [3, 4], sex [3–5], myocardial region (e.g., shorter T_2 in apical segments) [5, 6], T_2 mapping sequence (e.g., shorter T_2 with T_2 -prepared balanced steady state free precession [bSSFP] compared to gradient and spin echo (SE)) [6] and field strength (lower at 3 T) [6]. In the literature, the normal values for native myocardial T_2 in health have been provided as mean \pm 1 standard deviation (SD) (though a 95% reference range is approximately \pm 2 SD). Although there have been multiple attempts to establish age and sex corrected normal values for T_2 [3, 7, 8], currently no widely accepted reference ranges exist. Similarly, the myocardial T_2 values in inflammation are still debated, but they seem to lie in the \sim 55 to 74 ms interval at 1.5 T [2].

The T_1 Mapping and Extracellular Volume standardization (T1MES[®]) phantom [9] previously developed by our research group, provided a roadmap for developing a quality assurance medical device system for T_1 mapping and this has now been extensively validated [10]. Yet T1MES[®] was primarily a T_1 mapping phantom, designed to cover the range of blood and myocardial T_1 before and after the administration of gadolinium-based contrast agents (GBCA). Its T_2 coverage was therefore limited to just 6 T_2 values from 42 to 243 ms but none in the \sim 55 to 74 ms interval [9] meaning it provided a poor coverage of long native myocardial T_2 that we typically measure in the

acutely inflamed myocardium [2]. The use of T1MES[®] as a T_2 quality assurance device, is therefore hindered by the fact that it does not offer a granular enough representation of the relevant T_2 values across the health to inflammation spectrum (i.e., \sim 43 ms–74 ms). The hypertrophic cardiomyopathy registry (HCMR) phantom [11] was also designed for T_1 mapping and covers only two myocardial T_2 values (57 ms and 75 ms). Lastly, although the International Society of Magnetic Resonance in Medicine (ISMRM)/National Institute of Standards and Technology Laboratory (NIST) phantom [12] provides wide T_2 coverage with 14 vials spanning T_2 from 5 to 940 ms, only two of these are relevant for human myocardium (45 ms and 65 ms). Therefore, the existing CMR phantoms fall short of capturing clinically valid myocardial T_2 values meaning that the cardiovascular T_2 mapping community does not have a robust quality assurance reference object.

Using the collaboration and expertise gained through the T1MES[®] programme, we sought to design a T_2 mapping phantom that could be used interchangeably at both 1.5 T and 3 T, and that reflects clinically relevant native and post-GBCA T_2 in myocardium across the spectrum of health and disease.

Materials and methods

Collaboration process

The design collaboration has been previously described in the literature [9]. Briefly, it consisted of clinicians, physicists, national metrology institutes (the NIST and the German Physikalisch-Technische Bundesanstalt [PTB]) and a medium enterprise (the Australian Resonance Health [RH]).

Phantom and tube composition

Currently, there is no ideal material for phantom manufacture. As a first step, materials were filtered based on flow properties since fluid movement during imaging can introduce uncertainty in the T_2^* to T_2 conversion [13]. Given their viscosity, gels (e.g., agarose, gelatin, silicone, polyacrylamide, etc.) are preferable as they are not prone to fluid movement within an image slice during inversion recovery. Although the long-term stability of gels is limited because of gel contraction leading to gaps, we opted to use an agarose-based gel for phantom manufacture as this has been shown to be stable for 1–2 years [10,

14]. As microbial action can affect long-term stability, decontaminated high purity water was used. Although there are many available paramagnetic ions (e.g., copper, iron, manganese etc.), we chose nickel (Ni^{2+}) given its lesser dependence on frequency and temperature [15, 16]. Thus, our phantom was a diamagnetic matrix consisting of an agarose-gel (polysaccharide agarose powder with low endosmotic flow for electrophoresis, molar ratio ≤ 0.07 , Acros Organics) prepared with high purity deionized water (Ibis Technology) doped with paramagnetic nickel di-chloride (NiCl_2).

Each phantom contained 9 tubes (#60.9922.212, 30 ml from Sarstedt, Numbrecht, Germany) filled with the gel matrix described above (i.e., the inner matrix fill). The tubes were tightly screw-capped to prevent leaks. Since the concentration of the gelling agent [17] and the paramagnetic ion concentration [15] are inversely correlated with T_2 and T_1 ($T_1|T_2$) respectively, a gel tube with any required $T_1|T_2$ can be theoretically designed. The T_1 and T_2 interdependence of agarose and nickel has been previously described [9]. Briefly, different concentrations of NiCl_2 , agarose and water were prepared, transferred into preheated nuclear magnetic resonance (NMR) tubes (to avoid instant setting), allowed to set, analyzed at 22 °C using a non-imaging 1.4 T Bruker (Billerica, Massachusetts, USA) Minispec mq60 (60 MHz) relaxometer, and $T_1|T_2$ were recorded following exponential fitting. Assuming a linear relationship between ingredients and relaxation rates (i.e., $1/T_1$ and $1/T_2$) [18], the ingredients required for any $T_1|T_2$ tube could thus be calculated. Thus, 9 unique stock solutions were constructed

providing the clinically relevant native and post-GBCA $T_1|T_2$ tube combinations observed in myocardium across the spectrum of health and disease (Table 1). A detailed description of the linear models used for longitudinal and transverse relaxation rates in terms of the ingredients agarose and NiCl_2 , and of the exponential fitting has been previously published [9].

These 9 tubes were contained within a plastic bottle and the inter-tube space packed with the outer matrix fill which consisted of a similar NiCl_2 doped agarose-gel matrix as described above, but additionally containing high-density polyethylene (HDPE) beads. Regarding the choice of the outer matrix fill $T_1|T_2$ properties, we selected the combination that yielded the lowest bSSFP stabilization artefacts at both 1.5 T and 3 T based on B_1 uniformity experiments described below. We chose HDPE beads as compared to sodium chloride or other plastic microbeads as they were better at flattening the B_1 field (experiments previously reported [9]). Since HDPE beads have a similar diamagnetism to the gel, the beads do not impact the B_0 field.

Structural integrity

Gel integrity and aging were checked at baseline (i.e., on receipt of the phantom in the UK post manufacture in Australia) and at 12-months. This was through the manual inspection of localizers and a high-resolution, isotropic, three-dimensional (3D) gradient echo sequence (0.42mm^3) acquired on two Siemens CMR systems (Siemens Healthineers, Erlangen, Germany) at the University College London (UCL) Bloomsbury Center for

Table 1 Measured $T_1|T_2$ myocardial values for the 9 tubes and outer matrix fill

	T1 (ms)			T2 (ms)			Agarose (%)	Ni^{2+} (mM)
	1.4 T	1.5 T	3 T	1.4 T	1.5 T	3 T		
Short T_2 native myo at both 1.5 T and 3 T (A)	821	803	807	40	35	34	1.261	3.139
Medium T_2 native myo at 1.5 T (B)	978	982	988	50	43	41	0.969	2.511
Medium T_2 native myo at 3 T (C)	1122	1073	1137	48	42	40	0.773	2.639
Long T_2 native myo at 1.5 T (D)	1083	1090	1130	71	60	59	0.821	1.775
Long T_2 native myo at 3 T (E)	1237	1225	1228	70	61	59	0.649	1.791
Long-normal T_2 native myo at 1.5 T (F)	1030	1015	1019	60	52	50	0.882	2.081
Very long T_2 native myo at 3 T (G)	1295	1287	1302	82	70	68	0.594	1.562
Mildly long T_1 & T_2 native myo at 1.5 & 3 T (H)	1221	1182	1217	60	52	51	0.664	2.139
Medium T_1 & T_2 post-GBCA* myo at 1.5 & 3 T (I)	440	435	445	47	41	40	2.840	2.502
Outer gel matrix fill	850	-	-	140	-	-	1.155	0.780

All the $T_1|T_2$ presented in this table were measured in our final phantom ($n = 1$). $T_1|T_2$ at 1.4 T were measured by a Bruker minispec mq60 relaxometer (22 °C) at Resonance Health laboratory in Australia; T_1 and T_2 at 1.5 T and 3 T were measured by inversion recovery gradient echo and single-echo spin echo at University College London at baseline. The definitions of 'short', 'medium', 'long-normal', 'long', 'mildly long' and 'very long' are subjective and relative to the average normal native myocardial T_2 in health

* The post-contrast myocardial T_1 behavior being modelled here is based on the published literature around the use of Dotarem (Gadoterate meglumine, Guerbet, France) so the effects may not be generalizable to other GBCAs

GBCA gadolinium-based contrast agent; myo myocardium; ms, milliseconds

Clinical Phenotyping using Magnetom Aera 1.5 T operating VE11C-SP01 and Magnetom Prisma 3 T operating VE11C-SP01, both with 18-channel phased-array chest coils. The latter sequence acquired two overlapping slabs (due to scanner software constraints), each with two directions of phase encoding. It also had a long repetition time ($TR = 17$ ms) and narrow pixel bandwidth (250 Hz/pixel) for improved signal-to-noise ratio (SNR). This sequence had weak T_1 and T_2 image contrast and was only used for structural examination.

B_0 and B_1 uniformity

The phantom is composed of both paramagnetic constituents (such as Ni^{2+} that are attracted to B_0 because they have at least one unpaired electron) and diamagnetic constituents (such as agarose that are repelled by B_0 as all their electrons are paired). Since the concentration of Ni^{2+} is small, the paramagnetic effect of the phantom is $< 10\%$. Thus, the B_0 distortion caused by phantom components arises mainly from electronic diamagnetism. Although increasing the paramagnetic ion concentration would have counterbalanced the diamagnetism, this would have resulted in an excessive shortening of the relaxation times.

Regarding phantom design, the ideal shape would have been Lorentz uniform (e.g., ellipsoid body) to avoid

susceptibility-induced magnetostatic field perturbations, but such perfectly ellipsoidal geometry is difficult to mass produce. Although many phantoms are cylindrical, there are off-resonance artefacts even if the phantom is co-axially aligned with B_0 [19]. To compromise from a geometric point of view, our phantom's outer body shape along the z-axis was fairly ellipsoidal (Fig. 1i) but square in cross-section (Fig. 1ii) as it consisted of a rounded-edged, short, hollow, wide necked and leak-proof brown-transparent poly vinyl chloride (PVC) bottle with a melting temperature of $140^\circ C$. The volume of the phantom was 1 L, its length was 13 cm and inner body cross section was 10 cm by 10 cm. As the bottle base, cap and edges were prone to off-resonance errors, internal tubes were located near to the center of the bottle and fixed on top of a 20 mm layer of Epoxycast clear casting resin (Barnes, NSW, Australia). The choice of a resin layer height of 20 mm was guided by T_2 mapping bSSFP experiments which showed an off-resonance band compromising the lower 15 mm of the phantom body. To minimize field inhomogeneities at the bottle edges, tubes with long $T_1|T_2$ were arranged more centrally and avoided the corners. The physical length of the 9 $T_1|T_2$ tubes was the same. B_0 field uniformity as a measure of off-resonance at both 1.5 T and 3 T was mapped using a

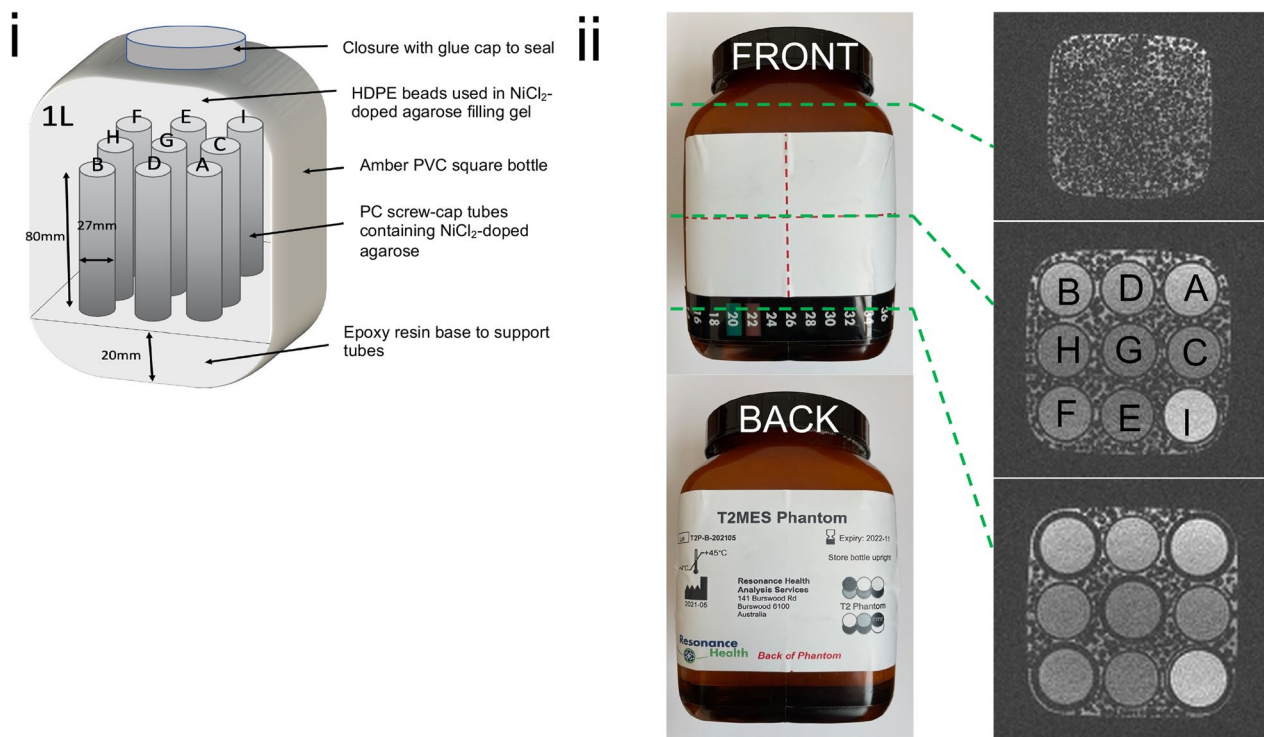


Fig. 1 i Schematic (not to scale) showing the internal and external phantom structure. ii Phantom front view showing isocenter line and liquid crystal display thermometer. HDPE = high-density polyethylene; PVC = polyvinyl chloride; PC = polycarbonate

single-echo gradient echo sequence, based on the phase difference between known echo times (TE) [20].

In the radiofrequency (RF) B_1 field, the water dipole moment rotates leading to displacement current. Using Maxwell's equations, the rate of the displaced current to conducted current is $Q = \frac{\omega\epsilon}{\sigma}$ (where ω is the angular frequency, ϵ is the permittivity and σ the conductivity). Thus, B_1 uniformity across the phantom body, could have been improved by either decreasing the permittivity or increasing the conductivity of the outer matrix fill. As per our previous work [9], we opted to decrease the permittivity and did so by densely packing oblate spheroidal HDPE beads (3 mm polar axis by 4.2 mm equatorial diameter) into the outer matrix fill. Each bead consisted of smooth, semi-translucent, colorless HDPE with a melting index > 60 °C (HDPE Marlex HHM 5502 BN, Chevron Phillips Chemical Company LP, Woodlands, Texas, USA). B_1 homogeneity was evaluated through flip angle (FA) maps derived by the double angle method (i.e., 60° and 120°) using short (i.e., 4 ms) sinc (-3π to $+3\pi$) slice excitation width via long TR (i.e., 8 s) scanning.

Reference T_1 and T_2

CMR studies on the T_2 phantom at baseline were performed using the 1.5 T Aera and 3 T Prisma (Siemens Healthineers) scanners at UCL. The scan protocol was identical for the two field strengths and consisted of inversion recovery (IR) gradient echo (GRE) for measuring reference T_1 (11 inversion times [ms]: 20, 50, 100, 200, 400, 600, 800, 1000, 1300, 1700, 2100; FA: 90°; TR: 10 s; resolution: 1.8 mm × 11.8 mm; slice thickness: 8 mm) and single-echo SE for measuring reference T_2 (10 TE [ms]: 10, 20, 30, 40, 50, 60, 80, 100, 125, 150; FA: 90°; TR: 10 s; resolution: 1.8 mm × 11.8 mm; slice thickness: 8 mm), both at 22 °C.

Temperature dependence of T_1 and T_2

Temperature dependency experiments on $T_1|T_2$ values were carried out at:

- *NIST* at 5 temperatures between 20.0 °C and 36.6 °C using an Agilent 3 T small bore scanner. T_1 was measured by IRSE (TR: 10 s; TI [ms]: 50, 75, 100, 125, 150, 250, 500, 1000, 1500, 2000, 3000, 6000) and T_2 by SE (TR: 10 s; TE [ms]: 14, 28, 56, 112);
- *PTB* at 6 temperatures between 13.5 °C and 38.8 °C using a 3 T Magnetom Verio system (VB17; Siemens Healthineers) and a 12-channel head coil. T_1 was measured by inversion recovery spin echo (IRSE, TR: 8 s; TI: 25–4800 ms) and T_2 by SE (TR: 3 s; TE: 24–400 ms).

At both centers, the scan resolution was 0.5 mm × 0.5 mm² and slice thickness was 2 mm. In addition, temperatures were measured using fiber optic probes.

Reproducibility

Short-term reproducibility experiments were performed using 3 repeats of T_1 mapping and T_2 mapping sequences on two final phantom prototypes (#Ci and #Cii) manufactured 12 months apart using independent stock solutions.

Long-term reproducibility experiments were performed to assess the variability of T_1 and T_2 measurements at baseline and at 12 months in one phantom (#Ci).

All tests were performed on the UCL 1.5 T and 3 T scanners both operating VE11A. T_1 mapping was by a 5 s(3 s)3 s 256-matrix RR=900 ms variant of modified Look-Locker inversion recovery (MOLLI) adapted for native T_1 mapping (1.5 T FA: 35°; 3 T FA: 20°; both Siemens WIP 1041B, acquired resolution: 1.4 mm × 1.9 mm and slice thickness: 8 mm). T_2 mapping was by a T_2 -prepared T_2 mapping sequence (bSSFP) at 1.5 T and 3 T (both FA: 70°; acquired resolution: 1.9 mm × 2.3 mm; slice thickness 8 mm). Each tube's $T_1|T_2$ were calculated in the reconstructed $T_1|T_2$ pixel-wise maps as the mean signal intensity values obtained from fixed diameter circular regions of interest (ROI) automatically placed in the central 50% radius of each tube. However, manual corrections were applied if appropriate to ensure optimal ROI centering in each tube.

Each scan session replicated the prescribed phantom set-up, with simulated electrocardiogram (ECG) at 67 beats per minute (ECG R-wave to R-wave interval: 900 ms). Details regarding the phantom position and adjustments before scanning, and phantom storage instructions can be found in the user manual (Additional file 1).

Statistical analysis

Statistical analysis was performed in R (version 4.0, R Foundation for Statistical Computing, Vienna, Austria). Curve fitting and ROI measurement was performed in MATLAB (R2020a, Mathworks, Natick, Massachusetts, USA). Distribution of data were assessed on histograms and normality checks were performed using the Shapiro–Wilk test. Continuous variables are expressed as mean ± 1 SD. Details for how we defined the model that describes the relation between ingredients and relaxation rates by fitting a surface for T_1 and T_2 , and using the linear least-squares approach, are provided in our previously published phantom work [9]. The

reproducibility between repeated scans was assessed through the coefficients of variation (CoV).

Results

Prototype testing and final phantom design

Three sequential prototypes (#A, #B, #C) were initially tested for B_0 and B_1 field inhomogeneities. Briefly, during the first two iterations (#A, #B), we reduced the bottle volume compared to TIMES[®] to reduce the artefacts and experimented with the use of 7 instead of 9 internal tubes arranged in a circular array (image not shown). However, this configuration was not stable and tube position shifts were observed after shipping, so the third and final prototype (#Ci) was constructed with a 3×3 array of 9 internal tubes, of slightly smaller diameter (24 mm) compared to TIMES[®]. Each center received a #Ci phantom, and provided quantitative and visual data for this manuscript. To study the reliability of manufacture and verify short-term reproducibility, another final prototype (#Cii) was manufactured 12 months after the manufacture of #Ci and sent to UCL to test the reliability of the production process having redone the 9 independent stock solutions.

A schematic representation of the phantom showing its internal and external structure is displayed in Fig. 1i. The actual phantom front and back views displaying cross-sectional slices of the isoelectric line, bottle cap and bottle base (above the epoxy resin base) are shown in Fig. 1ii. Tube arrangement is such that the more temperature-dependent and therefore unstable long- T_1 tubes are away from the corners and towards the middle of the 3×3 array.

Structural integrity

Inspection of localizers and high-resolution images acquired at baseline and at 12-months post manufacture, revealed no visible air bubbles, gel rips or tears down any of the tubes and images were free of susceptibility artefacts (Fig. 1iii and Additional file 2: Movie S1 and Additional file 3: Movie S2). This inspection was done visually by C.C.T. and G.C. T_1 and T_2 maps collected through the midline of the phantom, using the specified scan setup, were free from off-resonance artifacts.

Characterization of $T_1|T_2$ dependence on agarose and nickel

In the phantom, the $T_1|T_2$ measured on a 1.4 T Bruker relaxometer at 22 °C and on 1.5 T and 3 T clinical CMR systems using IRGRE, SE, MOLLI and T_2 mapping bSSFP are presented in Fig. 2i. Example T_1 and T_2 maps of the phantom are displayed in Fig. 2ii. The 9 compartments successfully covered the clinically meaningful range of native and post-GBCA myocardial T_2 in health and

disease (typically expected to be between 43 ms to 74 ms by T_2 mapping).

B_0 uniformity

When coaxially aligned with B_0 , scanning the phantom at its isocenter halfway along its length (i.e., scan slice-labelled on the phantom exterior) provided sufficient B_0 uniformity. The final phantom was free of off-resonance artifacts when scanned at the isocenter as per the user manual (i.e., bottle placed co-axial with the z axis, use of shimming etc.). Across the 9 tubes, off resonance at both 1.5 T and 3 T was less than 1 Hertz (Hz) (i.e., 0.008 parts per million [ppm] at 3 T or 0.004 ppm at 1.5 T) indicating minimal B_0 distortion. Given these are extremely small shifts, off resonance should not be considered as different between the 9 tubes. The associated 1.5 T and 3 T B_0 field maps are shown in Fig. 3i.

B_1 uniformity

Across the nine phantom compartments embedded in the outer matrix fill packed with HDPE beads, there was minimal B_1 field inhomogeneity as a measure of the FA (i.e., less than 0.9; exemplar 1.5 T and 3 T B_1 field maps in Fig. 3ii).

Reference $T_1|T_2$

Baseline reference T_1 obtained via IR GRE were compared to those obtained by pre-GBCA MOLLI T_1 mapping (Fig. 2i), while reference T_2 obtained via SE were compared with T_2 mapping bSSFP at both 1.5 T and 3 T for each of the 9 tubes Table 2 and Fig. 4.

Overall, there was a relatively good agreement between T_2 measured by T_2 mapping bSSFP and SE with a deviation of 6.3 ms [12.5%] at 1.5 T and 7.2 ms [14.7%] at 3 T. Corner tubes (i.e., A, B, F, and I) displayed a higher deviation at both 1.5 T (8.5 ms [19.9%] vs 4.9 ms [8.7%]) and 3 T (9.8 ms [23.6%] vs 5.5 ms [10.2%]). The difference is mostly driven by the post-GBCA ultra-low T_1 Tube I (that has a deviance of 15 ms [36.6%] and 16 ms [40.0%] for 1.5 T and 3 T respectively).

Temperature dependency

Temperature tests carried out at PTB and NIST in 3 T scanners, with T_1 was measured by IR SE, and T_2 by SE. As the temperature increases, T_1 increased and T_2 decreased across the 9 tubes (Fig. 5). Short and medium $T_1|T_2$ tubes were more stable as the variation in the temperature was more pronounced for long $T_1|T_2$ tubes (G, E, H, D).

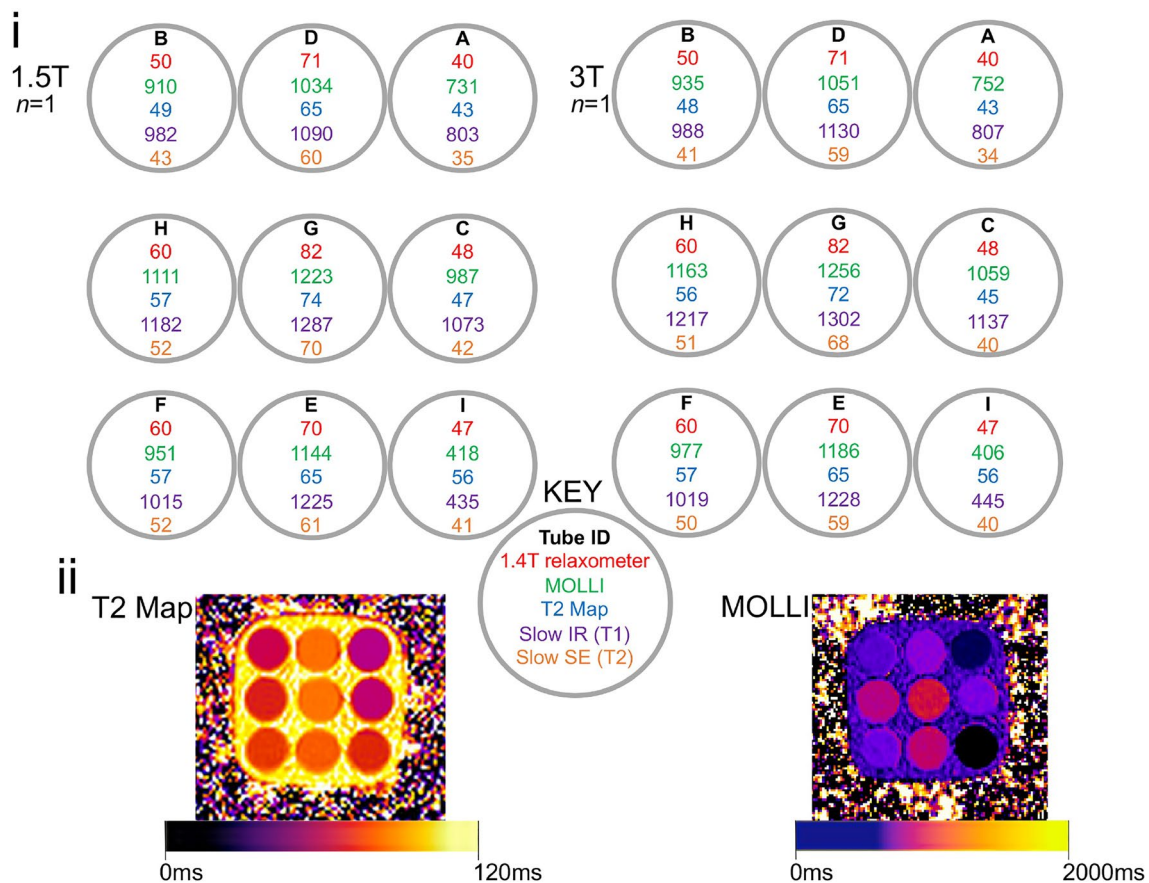


Fig. 2 i T₁ and T₂ (in ms) in the T₂ phantom (n = 1) as measured at 1.5 T and 3 T: slow scan reference T₁ obtained using inversion recovery (IR) gradient echo (GRE) (purple) and reference T₂ using single echo (SE) (orange); T₁ via modified Look-Locker inversion recovery (MOLLI) T₁ mapping (green) and T₂ via balanced steady state free precession (bSSFP) T₂ mapping (blue); T₂ obtained by the manufacturer in Australia using a 1.4 T Bruker minispec relaxometer at 22 °C (red). Tube arrangement is such that the more temperature-dependent and therefore unstable long-T₁ tubes are away from the corners and towards the middle of the 3 × 3 array. ii Exemplar T₂ and T₁ maps on a Siemens 3 T Prisma clinical CMR scanner. ID = tube identity

Reproducibility

Short-term reproducibility

All 9 tubes, at both field strengths, showed a CoV of < 1% for both T₁ and T₂ reproducibility, even in the absence of temperature correction, and regardless of phantom batch. As expected, tubes D and G with the longest T₁ and T₂ showed the greatest variability between repeated scans (Fig. 6).

Long-term reproducibility

Between the baseline and 12 month repeat scans, the CoV across all 9 tubes and both field strengths for T₁ measured by MOLLI T₁ mapping, was < 1.38% and for T₂ measured by bSSFP T₂ mapping was < 1.25% (range of CoV at 12 months for the 9 T₁ tubes at 1.5 T = 0.01–1.38% and at 3 T = 0.01–1.25%; range of CoV at 12 months for the 9 T₂ tubes at 1.5 T = 0.00–1.25% and at 3 T = 0.10–1.22%). All measurements were acquired

at 22 °C, meaning that no temperature correction was required. There was a greater variability of reads at 3 T compared to 1.5 T, and a greater variability of long T₁|T₂ tubes (D and G) compared to other tubes, in line with our previous work [10] (Table 3).

Discussion

In this study, we developed a T₂ phantom for quality assurance of T₂ mapping in CMR. By varying the concentrations of agarose and Ni²⁺ we were able to make 9 tubes that covered the relevant spectrum of human myocardial T₂ (i.e., both native and post-GBCA) across health and disease. At 12 months post manufacture compared to baseline, the phantom remained structurally intact and free of susceptibility artefacts when scanned at the isocenter, with good B₀ and B₁ field homogeneity and small variability in T₁|T₂ (all CoV < 1.38%).

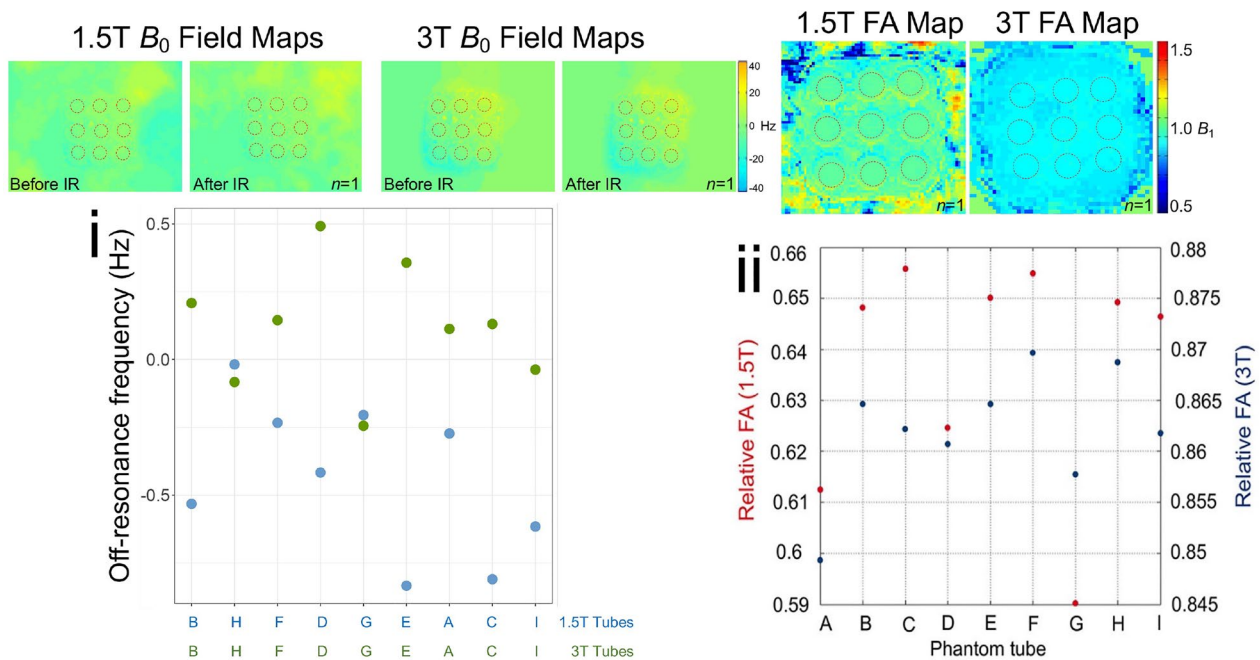


Fig. 3 i) B_0 field homogeneity across the nine phantom compartments as a measure of off-resonance in Hertz (Hz) at 1.5 T (blue) and 3 T (green) are shown (bottom). The associated B_0 field maps with the field of view capturing the whole phantom at 1.5 T and 3 T are also presented (top—tube positions are overlaid in red). ii) B_1 field homogeneity across the nine phantom compartments as a measure of the FA (in degrees) at 1.5 T (red) and 3 T (blue) are shown (bottom). These represent small shifts in FA or frequency (e.g., 10 Hz = 0.08 ppm at 3 T) and should not be regarded as significantly different between the tube compartments. As expected, the variation of relative FA is larger at 3 T (0.590–0.656) compared to 1.5 T (0.849–0.866). The associated B_1 field maps of at 1.5 T and 3 T are also presented (top—tube positions are overlaid in red). FA flip angle. Other abbreviations as in Fig. 2

Table 2 Comparison of T_2 obtained by reference (long-TR) spin-echo sequences versus balanced steady state free precession (bSSFP) T_2 mapping at 1.5 T (Siemens Aera) and 3 T (Siemens Prisma) on the final phantom ($n = 1$) at baseline

Biological scope (Tube ID)	1.5 T			3 T		
	T_2 mapping (ms)	Spin-Echo (ms)	Difference in ms (%)	T_2 mapping (ms)	Spin-Echo (ms)	Difference in ms (%)
Short T_2 native myocardium at both 1.5 T and 3 T (A)	43	35	8 (23%)	43	34	9 (27%)
Medium T_2 native myocardium at 1.5 T (B)	49	43	6 (14%)	48	41	7 (17%)
Medium T_2 native myocardium at 3 T (C)	47	42	5 (12%)	45	40	5 (13%)
Long T_2 native myocardium at 1.5 T (D)	65	60	5 (8%)	65	59	6 (10%)
Long T_2 native myocardium at 3 T (E)	65	61	4 (7%)	65	59	6 (10%)
Long-normal T_2 native myocardium at 1.5 T (F)	57	52	5 (10%)	57	50	7 (14%)
Very long T_2 native myocardium at 3 T (G)	74	70	4 (6%)	72	68	4 (6%)
Mildly long T_1 & T_2 native myocardium at 1.5 & 3 T (H)	57	52	5 (10%)	56	51	5 (10%)
Medium T_1 & T_2 post-GBCA* myocardium at 1.5 & 3 T (I)	56	41	15 (37%)	56	40	16 (40%)

Corner tubes are highlighted in bold

TR repetition time. Other abbreviations as in Table 1

T_2 mapping has gained a lot of traction lately as it enables both the visual identification and quantification

of regional and diffuse myocardial disease in a color-coded fashion [2]. T_2 mapping can be achieved using

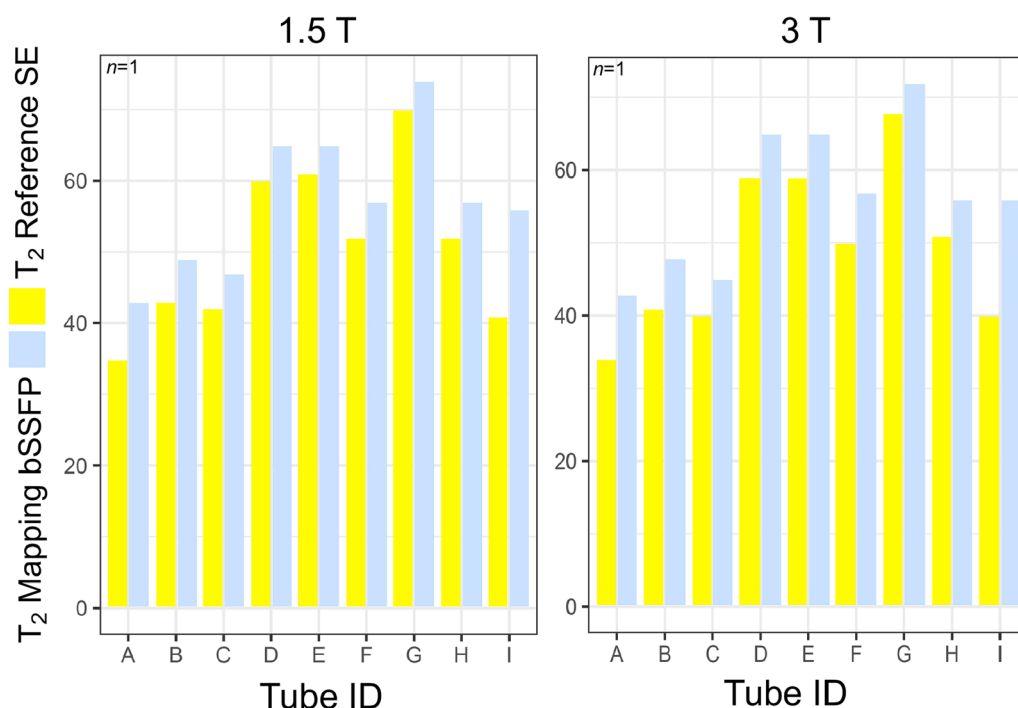


Fig. 4 Comparison of T_2 obtained by reference (long-TR) SE sequences (yellow) versus bSSFP T_2 mapping (grey) at 1.5 T (Siemens Aera, left) and 3 T (Siemens Prisma, right) on the final phantom ($n = 1$) at baseline. TR repetition time. Other abbreviations as in Fig. 2

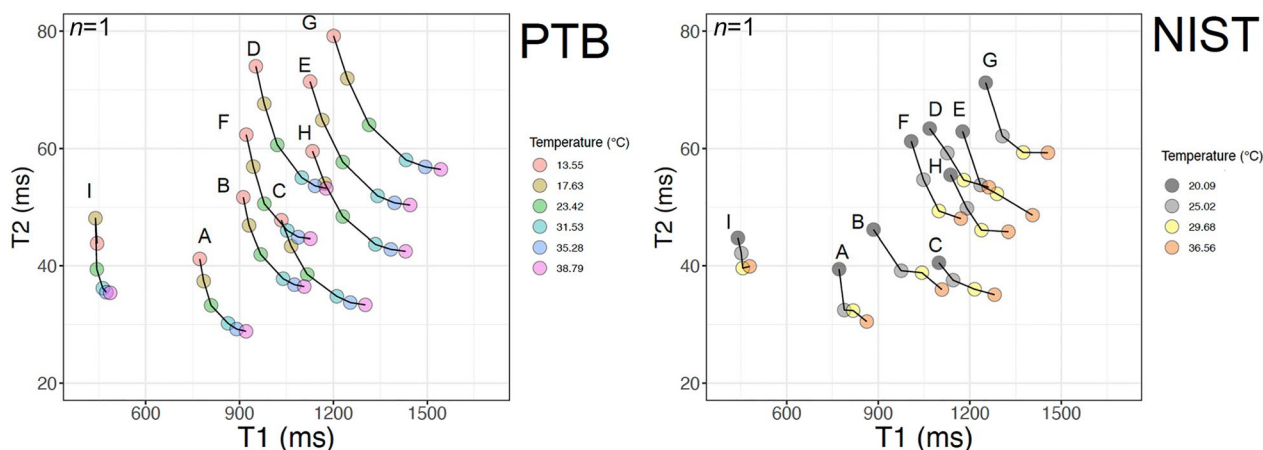


Fig. 5 Temperature tests carried out at PTB—German Physikalisch-Technische Bundesanstalt (left)—using a 3 T Siemens Magnetom Verio (VB17) and a 12-channel head coil and at NIST—US National Institute of Standards and Technology (right)—using an Agilent 3 T small bore scanner. T_1 was measured by IRSE, and T_2 by SE. The measurements were performed on the final phantom ($n = 1$) at baseline. TE Echo time. Other abbreviations as in Fig. 2

bright blood sequences such as turbo spin echo [21, 22], multi-echo spin echo [6], gradient spin echo [23], or T_2 -prepared bSSFP [24]. The latter is the most widely used given its accuracy [25] and reproducibility [26]. To overcome the inherent bias to T_1 of bSSFP, T_2 preparation (e.g., using the Carr-Purcell Malcom-Levit sequence [27]) can be employed to promote T_2 weighting (and hence the term T_2 -prepared bSSFP) [28]. Moreover,

T_2 -prepared sequences display a reduced field-strength variability [29]. Indeed, in our study the CoV were slightly higher at 3 T compared to 1.5 T.

To date, a gold standard calibration instrument for T_2 mapping is yet to be established. The design challenges which need to be considered when creating a phantom object for parametric mapping have been previously described [9]. Briefly, these include: (1) recipient shape

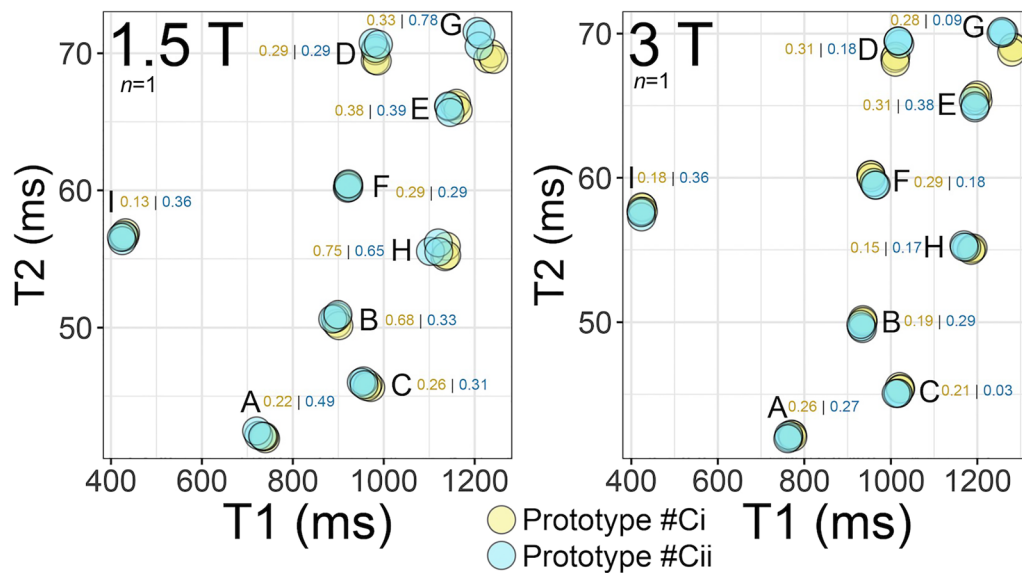


Fig. 6 Short-term reproducibility of T_2 at 1.5 T (left) and 3 T (right) acquired using T_2 mapping bSSFP repeated 3 times in each of the final prototypes #Ci (at a temperature of 22°) ($n = 1$) and #Cii (at 21°) ($n = 1$) manufactured months apart, from independent stock solutions. All these scans were performed on the same day with independent placement of phantom and shims. Coefficients of variation (CoV) of T_2 are shown per tube and were all < 1% in the absence of temperature correction. CoV for T_1 using 3 MOLLl repeats are not shown here but were also < 1% for both prototypes (1.5 T range: 0.13–0.94%; 3 T range: 0.03–0.38%)

Table 3 Long-term reproducibility results for one phantom at baseline and its 12 months repeat scan

Biological scope (Tube ID)	1.5 T $n = 1$		3 T $n = 1$	
	Baseline	12-month repeat (absolute difference in ms, % diff)	Baseline	12-month repeat (absolute difference in ms, % dif)
Short T_2 native myocardium at both 1.5 T and 3 T (A)	43	43 (0, 0%)	43	43 (0, 0%)
Medium T_2 native myocardium at 1.5 T (B)	49	49 (0, 0%)	48	49 (1, 2.1%)
Medium T_2 native myocardium at 3 T (C)	47	47 (0, 0%)	45	45 (0, 0%)
Long T_2 native myocardium at 1.5 T (D)	65	66 (1, 1.5%)	65	65 (0, 0%)
Long T_2 native myocardium at 3 T (E)	65	65 (0, 0%)	65	65 (0, 0%)
Long-normal T_2 native myocardium at 1.5 T (F)	57	57 (0, 0%)	57	57 (0, 0%)
Very long T_2 native myocardium at 3 T (G)	74	73 (1, 1.4%)	72	71 (1, 1.4%)
Mildly long T_1 & T_2 native myocardium at 1.5 & 3 T (H)	57	57 (0, 0%)	56	56 (0, 0%)
Medium T_1 & T_2 post-GBCA* myocardium at 1.5 & 3 T (I)	56	57 (1, 1.8%)	56	57 (1, 1.8%)

All the T_2 presented in this table were acquired using T_2 mapping bSSFP in final prototype #Ci at baseline and prototype #Cii at the 12-month repeat
Other abbreviations as in Table 2

magnetostatics and B_0 distortion, (2) long term stability, (3) structural considerations (e.g., seal, leakages, and air trapping), (4) adjustments of B_0 and reference frequency, (5) phantom diamagnetism, (6) in plane effects such as Gibbs artifact ringing, (5) field strength performance, (6) biological scope of selected $T_1|T_2$ (i.e., ideally covering clinically relevant pre/post-GBCA myocardial \pm blood values in health and disease), and (7) number of compartments and their arrangement. GBCA can

shorten both T_1 (~ 25%) and T_2 (~ 5%) [30], and T_2 mapping is usually done pre-GBCA [2]. However, we provisioned for one post-GBCA tube (tube I) on account of its potential research utility for groups working on pre- and post-GBCA multiparametric mapping and CMR fingerprinting. The current data suggest that the proposed CMR T_2 phantom has adequately addressed all these needs. This was enabled by the expertise gained from the recently completed T1MES® programme [10].

Compared to our T1MES[®] phantom, the CMR T₂ phantom: (1) provides improved coverage of the myocardial native and post-GBCA T₂ in health and disease, (2) is useable at both field-strengths for more flexible and cost-effective utilization by end users, and (3) has a smaller total volume compared to T1MES[®] to further reduce artefacts. Although the T₂ phantom covers *some* clinically relevant T₁ values, the T1MES[®] phantom provides a more extensive coverage of T₁ in health and disease, better field strength specificity and dedicated pre- and post-GBCA blood and myocardial T₁ tubes. Thus, if T₁ mapping/Extracellular Volume (ECV) quantification quality assurance is being pursued, we still recommend using the T1MES[®] phantom for such calibration, instead of the T₂ phantom.

Our T₂ phantom is partly composed of diamagnetic (the gel and HDPE beads) and paramagnetic (Ni²⁺) constituents, but since the Ni²⁺ concentrations are extremely small, the prevailing interaction of the device with the magnetic field may be considered to be diamagnetic causing a negligible frequency shift of <1 Hz (equivalent to <0.008 ppm). Based on our experience with T1MES[®], we expect the T₂ phantom to have a shelf-life of up to 2 years, but currently only a single final phantom has been tested and only up to 12 months.

Based on published cohort studies, 1 SD of the mean native myocardial T₂ is generally ~3 ms at 1.5 T and 3 T [31–33]. Thus, we arbitrarily pre-defined as repeatable (and suitable for clinical/research use), a phantom object where the estimated variance of its serial T₂ data did not exceed ½ of the above 1 SD. Assuming a typical native myocardial T₂ of 45 ms and a variance of ≤1.5 ms (i.e., ½ of the mean native myocardial T₂), this yields an acceptable CoV ≤2.7%. We go on to show that the long-term (12-month) reproducibility of the CMR T₂ phantom was in fact of the order <1.38% (and short-term reproducibility <1%) when using CoV.

All tubes regardless of whether they have a central or corner position express similar deviances of bSSFP T₂ compared to SE T₂ except for post-GBCA Tube I (which has a deviance of 15 ms [36.6%] at 1.5 T and 16 ms [40.0%] at 3 T). Tube I's extreme bSSFP vs SE deviances are partly due to its ultra-low T₁ (406 ms) which differentially impacts T₂ reads by bSSFP vs SE sequences. For the remaining 8 tubes, measurement errors between SE and bSSFP T₂ tended to be slightly higher in corner when compared to central tubes, at both 1.5 T (6.3 ms [11.5%] vs 4.9 ms [8.7%]) and 3 T (8 [16.2%] vs 5.5 ms [10.2%]).

Moving forward, we anticipate our CMR T₂ mapping phantom will be able to support multi-center T₂ mapping studies by allowing sites to measure and compare the stabilities of their local sequence-software combinations and permit comparisons across centres for the pooling

data. By highlighting performance discrepancies between T₂ mapping prototypes and established commercially available products, developers will be compelled to refine their sequences if appropriate, thus advancing the T₂ mapping field. In addition, we also expect our phantom to pave the way towards local phantom calibration overriding the need for local reference ranges [34].

A mandatory step before transitioning this device into clinical CMR centers for local quality assurance, is the receipt of regulatory clearance. Our applications for clearance by the US Food and Drug Administration (FDA), Conformité-Europeen (CE) mark in the EU and Therapeutic Goods Administration (TGA) in Australia are in progress.

Limitations

A limitation of our study is that the number of phantoms tested (i.e., four) was small. Stability was evaluated in one phantom, and reproducibility and accuracy were evaluated in two at a single center, of which one was at 1.5 T and one was at 3 T.

Phantoms have an unrealistically high SNR, are not magnetically representative of tissues as they fail to embody properties such as magnetization transfer, and they do not capture clinically relevant CMR challenges such as partial volume effects at the blood-myocardial interfaces [9, 10, 35]. These factors were beyond the scope of our study which aimed solely to pilot a quality assurance T₂ mapping phantom. In addition, good in vitro performance in phantom experiments does not guarantee good performance in patients as it fails to capture real-life clinical scenarios (e.g., patients with arrhythmias). The temperature sensitivity of the tubes might be problematic in severely hypo- or hyperthermic patients. All the CMR imaging was performed using a single vendor (Siemens) at UCL. The standard Siemens color scale for the T₂ map was noted to be insufficiently granular within the physiological range. GBCA can shorten both T₁ (~25%) and T₂ (~5%) [30], but the effects vary based on the specific GBCA used. Studying individual GBCA agents was beyond the scope of this study. Higher concentrations of the paramagnetic Ni²⁺ would have been required to capture physiologically relevant T₂^{*} at the cost of B₀ distortion. As this would have reduced our ability to model T₂, quality assurance of T₂^{*} mapping was not pursued in this work.

The overall purpose of phantoms is to create a reproducible set of T₁|T₂ that can be used to calibrate imaging sequences within a site longitudinally and at different sites. In this paper, we defined adequacy in terms of B₀|B₁ uniformity and T₁|T₂ precision rather than T₁|T₂ accuracy, given the known differences between SE and bSSFP or other vendor-specific T₂ mapping

readouts, particularly in the context of varying tube- T_1 and temperature. Given myocardial T_2 ranges from about 43 to 74 ms in health, the average absolute deviations between SE and T_2 bSSFP (i.e., 6.3 ms at 1.5 T and 7.2 ms at 3 T) represent $\sim 20\%$ of the physiological range except for the ultra-low T_1 tube I whose deviation represents $\sim 50\%$. When evaluating accuracy, focusing solely on the absolute difference in ms between T_2 measured by T_2 mapping bSSFP and SE can be misleading. However, percentage differences are also provided. A cylindrical phantom with greater edges-tubes spacing may have led to a better $T_1|T_2$ accuracy but this would have been associated with more off-resonance artefacts. Although the 9 stock solutions for tubes are reproducibly specified, slight inter-batch differences are to be expected as with all nickel-chloride/agarose solutions, even when formulated using rigorous protocols. This is why each new stock solution, undergoes de novo 1.4 T Bruker relaxometer at source, meaning these T_1 and T_2 values can be shared with the receiving centres to serve as a benchmark for cross-site comparisons between batches. Lastly, inter-center reproducibility was not addressed, and the reported short and long-term reproducibility data were based on single-centre results from one final T_2 phantom serially examined at UCL. Since it is of vital importance in the phantom's transition to clinical practice, this will be the focus of our future work.

Conclusion

We have reported on the development and testing of a T_2 mapping phantom demonstrating good structural integrity, B_0/B_1 uniformity, reproducibility and coverage of the clinically relevant myocardial $T_1|T_2$ across health and disease. This device may now be mass-produced to support the quality assurance of T_2 mapping in clinical and research practice.

Abbreviations

bSSFP	Balanced steady state free precession
CMR	Cardiovascular magnetic resonance
ECG	Electrocardiogram
FA	Flip angle
GBCA	Gadolinium based contrast agent
GRE	Gradient echo
HDPE	High-density polyethylene
IR	Inversion recovery
MOLLI	Modified Look-Locker inversion recovery
NIST	National Institute of Standards and Technology Laboratory
PC	Polycarbonate
PTB	Physikalisch-Technische Bundesanstalt
PVC	Polyvinyl chloride
RF	Radiofrequency
SCMR	Society for Cardiovascular Magnetic Resonance
SE	Spin echo
T1MES	T1 Mapping and Extracellular Volume standardization
TE	Echo time

Supplementary Information

The online version contains supplementary material available at <https://doi.org/10.1186/s12968-023-00926-z>.

Additional file 1. T2 phantom for quality assurance of T2 mapping user manual.

Additional file 2: Movie S1. High-resolution imaging of the T2 phantom at baseline and at one-year post-manufacture at 1.5 T revealed no visible air bubbles, gel rips or tears down any of the tubes and images were free of susceptibility artefacts.

Additional file 3: Movie S2. High-resolution imaging of the T2 phantom at baseline and at one-year post-manufacture at 3 T revealed no visible air bubbles, gel rips or tears down any of the tubes and images were free of susceptibility artefacts.

Acknowledgements

The authors are indebted to all the staff of Resonance Health and to scientists and physicists at UCL Bloomsbury Center for Clinical Phenotyping. Dr. Andrew Arai served as the *JCMR* Guest Editor for this manuscript.

Author contributions

GC and JCM developed the concept and approach. IP and PK provided crucial scientific advice, computational scripts and graphical user interfaces that permitted data analysis. CCT, MF, HS, GC, and IP performed phantom design experiments in London and the statistical analysis. PK, KEK, KFS, RBr, BI, RN and KS performed phantom experiments on prototypes in the expert centers, participated in data interpretation, study design, and contributed to the manuscript; all authors reviewed and approved the final manuscript. CCT and GC wrote the manuscript and critically appraised the results. GC is the guarantor of this work, and she attests that all listed authors meet the authorship criteria and that no others meeting the criteria have been omitted. All authors were involved in critically reviewing and revising the manuscript, approved the final version as submitted and agree to be accountable for all aspects of the work. All authors read and approved the final manuscript.

Funding

This work was directly supported by the UCL National Institute of Health Research (NIHR) Biomedical Research Center (BRC) and a British Heart Foundation (BHF) infrastructure award (IG/18/5/33958). G.C. is supported by the BHF Special Programme Grant (SP/20/2/34841). J.C.M. is directly and indirectly supported by the UCL Hospitals NIHR BRC and Biomedical Research Unit at Barts Hospital respectively. G.C. and J.C.M. are supported by the Barts Charity HeartOME1000 project grant (MGU0427 / G-001411). A.H. receives support from the BHF, the Economic and Social Research Council (ESRC), the Horizon 2020 Framework Programme of the European Union, the National Institute on Aging, the NIHR University College London Hospitals BRC, the UK Medical Research Council and works in a unit that receives support from the UK Medical Research Council.

None of the funders was involved in study design, the collection, analysis, and interpretation of the data, or in the decision to submit the article for publication.

Availability of data and materials

The supplementary material provided contains detailed information about the T_2 mapping phantom set-up, use and analysis. Sequence protocols are available on GitHub (<https://github.com/gcaptur/T2-Mapping-for-CMR>).

Declarations

Ethics approval and consent to participate

An ethical approval waiver was applied, and no consent was required as this study did not involve the scanning or recruitment of human participants. However, all procedures performed were in accordance with the ethical standards of the institutional and/or national research committee and with the 1964 Helsinki declaration and its later amendments or comparable ethical standards.

Consent for publication

Not applicable.

Competing interests

The views expressed in this article are those of the authors who declare that they have no conflict of interest (financial or non-financial). W.P. is an employee of Resonance Health which is a medium commercial corporation.

Author details

¹Barts Heart Center, Barts Health NHS Trust, West Smithfield, London EC1A 7BE, UK. ²Institute of Cardiovascular Science, University College London, Huntley Street, London WC1E 6DD, UK. ³UCL Medical School, 74 Huntley Street, London WC1E 6DE, UK. ⁴Department of Cardiology, Center for Inherited Heart Muscle Conditions, Royal Free London NHS Foundation Trust, Pond Street, London NW3 2QG, UK. ⁵Medical Research Council Unit for Lifelong Health and Ageing at UCL, 1-19 Torrington Place, London WC1E 7HB, UK. ⁶National Institute of Standards and Technology (NIST), 325 Broadway, Boulder, CO 80305, USA. ⁷Physikalisch-Technische Bundesanstalt (PTB), Abbestraße 2-12, 10587 Berlin, Germany. ⁸UCL Bloomsbury Center for Clinical Phenotyping, London WC1E 6HX, UK. ⁹Resonance Health (RH), 141 Burswood Road, Burswood, WA 6100, Australia. ¹⁰Department of Medicine (Cardiovascular Division), Beth Israel Deaconess Medical Center, Harvard Medical School, 330 Brookline Ave, Boston, MA 02215, USA. ¹¹National Heart, Lung and Blood Institute, National Institutes of Health (NIH), Rockville Pike, Bethesda, MD 20892, USA. ¹²Institute of Cardiovascular Science, Consultant Cardiologist in Inherited Heart Muscle Conditions, University College London, Gower Street, London WC1E 6BT, UK.

Received: 19 August 2022 Accepted: 26 January 2023

Published online: 20 March 2023

References

- Moon JC, Messroghli DR, Kellman P, Piechnik SK, Robson MD, Ugander M, Gatehouse PD, Arai AE, Friedrich MG, Neubauer S, et al. Myocardial T1 mapping and extracellular volume quantification: A Society for Cardiovascular Magnetic Resonance (SCMR) and CMR Working Group of the European Society of Cardiology consensus statement. *J Cardiovasc Magn Reson*. 2013;15:92–92. <https://doi.org/10.1186/1532-429X-15-92>.
- Topriceanu C-C, Pierce I, Moon J, Captur G. T₂ and T₂* mapping and weighted imaging in cardiac MRI. In: *Magnetic Resonance Imaging*; 2022:15–32.
- Roy C, Slimani A, De Meester C, Amzulescu M, Pasquet A, Vancraeynest D, Vanoverschelde J-L, Pouleur A-C, Gerber BL. Age and sex corrected normal reference values of T1, T2, T2* and ECV in healthy subjects at 3T CMR. *J Cardiovasc Magn Reson*. 2017;19:72–72. <https://doi.org/10.1186/s12968-017-0371-5>.
- Granitz M, Motloch LJ, Granitz C, Meissnitzer M, Hitzl W, Hergan K, Schlattau A. Comparison of native myocardial T1 and T2 mapping at 1.5T and 3T in healthy volunteers: Reference values and clinical implications. *Wien Klin Wochenschr*. 2018;131:143–55. <https://doi.org/10.1007/s00508-018-1411-3>.
- Wiesmueller M, Wuest W, Heiss R, Treutlein C, Uder M, May MS. Cardiac T2 mapping: Robustness and homogeneity of standardized in-line analysis. *J Cardiovasc Magn Reson*. 2020;22:39–39. <https://doi.org/10.1186/s12968-020-00619-x>.
- Baeßler B, Schaarschmidt F, Stehning C, Schnackenburg B, Maintz D, Bunck AC. A systematic evaluation of three different cardiac T2-mapping sequences at 1.5 and 3T in healthy volunteers. *Eur J Radiol*. 2015;84:2161–70. <https://doi.org/10.1016/j.ejrad.2015.08.002>.
- Von Knobelsdorff-Brenkenhoff F, Prothmann M, Dieringer MA, Wassmuth R, Greiser A, Schwenke C, Niendorf T, Schulz-Menger J. Myocardial T1 and T2 mapping at 3 T: Reference values, influencing factors and implications. *J Cardiovasc Magn Reson*. 2013;15:53–53. <https://doi.org/10.1186/1532-429X-15-53>.
- Snel GJH, van den Boomen M, Hernandez LM, Nguyen CT, Sosnovik DE, Velthuis BK, Slart RHJA, Borra RJH, Prakken NHJ. Cardiovascular magnetic resonance native T2 and T2 quantitative values for cardiomyopathies and heart transplantations: a systematic review and meta-analysis. *J Cardiovasc Magn Reson*. 2020;22:34–34. <https://doi.org/10.1186/s12968-020-00627-x>.
- Captur G, Gatehouse P, Keenan KE, Heslinga FG, Bruehl R, Prothmann M, Graves MJ, Eames RJ, Torlasco C, Benedetti G, et al. A medical device-grade T1 and ECV phantom for global T1 mapping quality assurance - the T1 Mapping and ECV Standardization in cardiovascular magnetic resonance (T1MES) program. *J Cardiovasc Magn Reson*. 2016;18:1–20. <https://doi.org/10.1186/s12968-016-0280-z>.
- Captur G, Bhandari A, Brühl R, Ittermann B, Keenan KE, Yang Y, Eames RJ, Benedetti G, Torlasco C, Ricketts L, et al. T1 mapping performance and measurement repeatability: results from the multi-national T1 mapping standardization phantom program (T1MES). *J Cardiovasc Magn Reson*. 2020;22(1):31.
- Kramer CMMD, Appelbaum EMD, Desai MYMD, Desvigne-Nickens PMD, DiMarco JPM, Friedrich MGMD, Geller NP, Heckler SBA, Ho CYMD, Jerosch-Herold MP, et al. Hypertrophic Cardiomyopathy Registry: The rationale and design of an international, observational study of hypertrophic cardiomyopathy. *Am Heart J*. 2015;170:223–230. doi: <https://doi.org/10.1016/j.ahj.2015.05.013>
- Keenan K, Stupic K, Horneber E, Boss M, Russek S. Paramagnetic Ion Phantom to Independently Tune T1 and T2. In: *ISMRM 23rd Annu Meet Exhib: Abstract*; 2015.
- Keenan K, Stupic K, Horneber E, Boss M, Russek S. Paramagnetic Ion Phantom to Independently Tune T1 and T2. In: *ISMRM 23rd Annual Meet Exhib. 2015, Abstract*; 2015.
- Vassiliou V, Heng EL, Donovan J, Greiser A, Babu-Narayan SV, Gatzoulis MA, Firmin D, Pennell DJ, Gatehouse P, Prasad SK. Longitudinal stability of gel T1 MRI Phantoms for quality assurance of T1 mapping. *J Cardiovasc Magn Reson*. 2015;17:1–3. <https://doi.org/10.1186/1532-429X-17-S1-W28>.
- Kraft KA, Fatouros PP, Clarke GD, Kishore PRS. An MRI phantom material for quantitative relaxometry. *Magn Reson Med*. 1987;5:555–62. <https://doi.org/10.1002/mrm.1910050606>.
- Koenig SH, Brown IJ RD. Relaxation of solvent protons by paramagnetic ions and its dependence on magnetic field and chemical environment: implications for NMR imaging. *Magn Reson Med*. 1984;1:478–95. <https://doi.org/10.1002/mrm.1910010407>.
- Mitchell MD, Kundel HL, Axel L, Joseph PM. Agarose as a tissue equivalent phantom material for NMR imaging. *Magn Reson Imaging*. 1986;4:263–6. [https://doi.org/10.1016/0730-725X\(86\)91068-4](https://doi.org/10.1016/0730-725X(86)91068-4).
- Yoshida A, Kato H, Kuroda M, Hanamoto K, Yoshimura K, Shibuya K, Kawasaki S, Tsunoda M, Kanazawa S, Hiraki Y. Development of a phantom compatible for MRI and hyperthermia using carrageenan gel-relationship between T1 and T2 values and NaCl concentration. *Int J Hyperth*. 2004;20:803–14. <https://doi.org/10.1080/0265673042000199268>.
- Ferreira PF, Gatehouse PD, Mohiaddin RH, Firmin DN. Cardiovascular magnetic resonance artefacts. *J Cardiovasc Magn Reson*. 2013;15:41–41. <https://doi.org/10.1186/1532-429X-15-41>.
- Hernando D, Kellman P, Halder JP, Liang ZP. Robust water/fat separation in the presence of large field inhomogeneities using a graph cut algorithm. *Magn Reson Med*. 2010;63:79–90. <https://doi.org/10.1002/mrm.22177>.
- He T, Gatehouse PD, Anderson LJ, Tanner M, Keegan J, Pennell DJ, Firmin DN. Development of a novel optimized breathhold technique for myocardial T2 measurement in thalassemia. *J Magn Reson Imaging*. 2006;24:580–5. <https://doi.org/10.1002/jmri.20681>.
- Kim D, Jensen JH, Wu EX, Sheth SS, Brittenham GM. Breathhold multiecho fast spin-echo pulse sequence for accurate R2 measurement in the heart and liver. *Magn Reson Med*. 2009;62:300–6. <https://doi.org/10.1002/mrm.22047>.
- Oshio K, Feinberg DA. GRASE (Gradient-and Spin-Echo) imaging: A novel fast MRI technique. *Magn Reson Med*. 1991;20:344–9. <https://doi.org/10.1002/mrm.1910200219>.
- Salerno M, Kramer CM. Advances in Parametric Mapping with Cardiac Magnetic Resonance Imaging. *JACC Cardiovasc Imaging*. 2013;6:806–22. <https://doi.org/10.1016/j.jcmg.2013.05.005>.
- Giri S, Chung Y-C, Merchant A, Mihai G, Rajagopalan S, Raman SV, Simonetti OP. T2 quantification for improved detection of myocardial edema. *J Cardiovasc Magn Reson*. 2009;11:56–56. <https://doi.org/10.1186/1532-429X-11-56>.
- Baessler B, Schaarschmidt F, Schnackenburg B, Stehning C, Giolda AD, Maintz D, Bunck A. Reproducibility of three different cardiac T2-mapping sequences at 1.5T and impact of cofactors on T2-relaxation times. *J Cardiovasc Magn Reson*. 2015;17:1–2. <https://doi.org/10.1186/1532-429X-17-S1-W12>.

27. Levitt MH, Freeman R. Compensation for pulse imperfections in NMR spin-echo experiments. *J Magn Reson*. 1969;1981(43):65–80. [https://doi.org/10.1016/0022-2364\(81\)90082-2](https://doi.org/10.1016/0022-2364(81)90082-2).
28. Chavhan GB, Babyn PS, Jankharia BG, Cheng HLM, Shroff MM. Steady-state MR imaging sequences: physics, classification, and clinical applications. *Radiographics*. 2008;28:1147–60. <https://doi.org/10.1148/rg.284075031>.
29. Hanson CA, Kamath A, Gottbrecht M, Ibrahim S, Salerno M. T2 relaxation times at cardiac MRI in healthy adults: A systematic review and meta-analysis. *Radiology*. 2020;297:344–51. <https://doi.org/10.1148/RADIOL.2020200989>.
30. Rohrer M, Bauer H, Mintonovitch J, Requardt M, Weinmann H-J. Comparison of Magnetic Properties of MRI contrast media solutions at different magnetic field strengths. *Invest Radiol*. 2005;40:715–24. <https://doi.org/10.1097/01.rli.0000184756.66360.d3>.
31. Ridouani F, Damy T, Tacher V, Derbel H, Legou F, Sifaoui I, Audureau E, Bodez D, Rahmouni A, Deux J-F. Myocardial native T2 measurement to differentiate light-chain and transthyretin cardiac amyloidosis and assess prognosis. *J Cardiovasc Magn Reson*. 2018;20:58–58. <https://doi.org/10.1186/s12968-018-0478-3>.
32. Kawel-Boehm N, Hetzel SJ, Ambale-Venkatesh B, Captur G, Francois CJ, Jerosch-Herold M, Salerno M, Teague SD, Valsangiacomo-Buechel E, van der Geest RJ, et al. Reference ranges ("normal values") for cardiovascular magnetic resonance (CMR) in adults and children: 2020 update. 2020.
33. Montant P, Sigovan M, Revel D, Douek P. MR imaging assessment of myocardial edema with T2 mapping. *Diagn Interv Imaging*. 2015;96:885–90. <https://doi.org/10.1016/j.diii.2014.07.008>.
34. Messroghli DR, Moon JC, Ferreira VM, Grosse-Wortmann L, He T, Kellman P, Mascherbauer J, Nezafat R, Salerno M, Schelbert EB, et al. *J Cardiovasc Magn Reson*. 2017;19(75):2017.
35. McGarry CK, Grattan LJ, Ivory AM, Leek F, Liney GP, Liu Y, Miloro P, Rai R, Robinson AP, Shih AJ, et al. Tissue mimicking materials for imaging and therapy phantoms: a review. 2020.

Publisher's Note

Springer Nature remains neutral with regard to jurisdictional claims in published maps and institutional affiliations.

Ready to submit your research? Choose BMC and benefit from:

- fast, convenient online submission
- thorough peer review by experienced researchers in your field
- rapid publication on acceptance
- support for research data, including large and complex data types
- gold Open Access which fosters wider collaboration and increased citations
- maximum visibility for your research: over 100M website views per year

At BMC, research is always in progress.

Learn more biomedcentral.com/submissions

